PAPER

Non-gravitational signals of dark energy under a gauge symmetry

Journal of Cosmology and Astroparticle Physics
An IOP and SISSA journal

Received: *December 23, 2023*
Revised: *January 26, 2024*
Accepted: *February 13, 2024*
Published: *March 21, 2024*

Non-gravitational signals of dark energy under a gauge symmetry

Kunio Kaneta,[a] **Hye-Sung Lee**,[b] **Jiheon Lee**[b] **and Jaeok Yi**[b]

[a]*Department of Physics, Osaka University, Toyonaka, Osaka 560-0043, Japan*
[b]*Department of Physics, Korea Advanced Institute of Science and Technology, Daejeon 34141, Korea*

E-mail: kaneta@het.phys.sci.osaka-u.ac.jp, hyesung.lee@kaist.ac.kr, anffl0101@kaist.ac.kr, wodhr1541@kaist.ac.kr

Abstract: We investigate non-gravitational signals of dark energy within the framework of gauge symmetry in the dark energy sector. Traditionally, dark energy has been primarily studied through gravitational effects within general relativity or its extensions. On the other hand, the gauge principles have played a central role in the standard model sector and dark matter sector. If the dark energy field operates under a gauge symmetry, it introduces the possibility of studying all major components of the present universe under the same gauge principle. This approach marks a significant shift from conventional methodologies, offering a new avenue to explore dark energy.

Keywords: dark energy theory, particle physics - cosmology connection

ArXiv ePrint: 2312.09717

https://doi.org/10.1088/1475-7516/2024/03/048

JCAP03(2024)048

Contents

1 Introduction

The Nobel prize-won discovery that the universe is in an accelerated expansion [1, 2] indicates the existence of the illusive component with negative pressure called dark energy. Although dark energy constitutes the majority of the energy density of the present universe, the confirmed influence of dark energy is limited to the narrow era of the recent universe through the Hubble expansion. Therefore, it remains one of the vaguest parts of cosmology, where further studies are warranted.

One of the well-known dark energy models is the quintessence field [3–6]. The quintessence field model describes dark energy as a homogeneous scalar field rolling down the potential. It can generate an accelerated expansion in a similar way that the inflaton field generates the primordial inflation of the universe, one of the most promising scenarios for the early universe.[1] Reflecting the fertile physics of inflaton, we are naturally led to consider that a scalar field may exist behind the present-day expansion of the universe.

There are indeed many ultraviolet theories that imply the existence of light scalars, such as dilatons [13–15], axions [16, 17], and other scalar degrees of freedom in extended theories [18–33]. One such particle may be identified as the quintessence field. The observation of cosmic microwave background (CMB) [34] gives the present energy density of the quintessence field as tiny as $10^{-47}\,\mathrm{GeV}^4$, whereas the value could have been different in the early universe. The

[1] However, see, for instance, ref. [7] for alternative scenarios. Extensive studies on the inflationary models have figured out that the inflaton can also provide the seeds for the structure formation [8, 9] or generate the heat bath needed for the big bang nucleosynthesis (BBN) [10–12].

JCAP03(2024)048

energy density of the quintessence field is determined by the field evolution throughout the thermal history of the universe. Therefore, it could be the case that cosmological events can be affected by the quintessence field dynamics in a different way than merely introducing the cosmological constant in theories. For instance, the quintessence field may address the cosmological coincidence problem by its nontrivial dynamics [35].

Since the standard model (SM) is built upon gauge symmetries, it is natural to suppose that dark energy may also have a gauge symmetry. In our previous works [36, 37], we suggested and investigated the "gauged quintessence" model where the quintessence field is charged under a new U(1) gauge symmetry. Due to the interaction between the gauge boson of the new gauge symmetry and the quintessence field, this model allows rich phenomenology. We showed that the gauged quintessence model may alleviate the Hubble tension issue suffered greatly by the original quintessence field model [38, 39], and could produce sizable relic vector density though the misalignment mechanism which is strongly suppressed in the minimal vector misalignment [40].

In this paper, we study non-gravitational signals in the gauged quintessence model. The dark energy sector may have a connection to the SM sector via the portals, the idea widely used in dark matter physics. Since the model has two components, that is, a vector boson and a scalar, one may use a vector portal (kinetic mixing between the hypercharge vector boson and the dark gauge boson) and/or a Higgs portal (mixing between the SM Higgs doublet and the quintessence field scalar). We will limit ourselves to only the vector portal in this paper. There has been discussion of non-gravitational signals of dark energy in various contexts. For instance, variation of the fundamental constants [41, 42], interaction to the matters [43, 44], interaction to the light relic [45, 46], laboratory experiments [47–50], and collider [51–55]. Our study differs in the sense that we use the gauge principle in studying dark energy à la many dark matter studies using the same principle. We will demonstrate how dark energy can influence the production of the dark gauge boson, and induce various observational astrophysical signals.

This paper is organized as follows. In section 2, we introduce the basic formalism of the gauged quintessence model with the kinetic mixing. In section 3, we discuss the production and decay of the dark gauge boson through kinetic mixing, and how they differ from the conventional dark photon model. In the subsequent sections, we discuss the constraints on our scenario from overproduction of the dark gauge boson, CMB distortion, diffuse X-ray/gamma-ray background, and distinguishable non-gravitational signals. We summarize and conclude in section 6.

2 Gauged quintessence model with kinetic mixing

The gauged quintessence model [36] includes a complex scalar Φ and a $\mathrm{U}(1)_{\mathrm{dark}}$ gauge boson $\hat{X}_\mu$. The complex scalar is charged under $\mathrm{U}(1)_{\mathrm{dark}}$ gauge symmetry, the radial part of Φ is taken as the quintessence field (ϕ), and the dark gauge boson gets the mass proportional to ϕ. As the quintessence field ϕ value evolves, $\hat{X}$ has a mass-varying characteristic. (For some other examples of the mass-varying particles, see refs. [56–65].)

JCAP03(2024)048

The dark gauge boson and SM hypercharge boson ($\hat{B}_\mu$) can be mixed via kinetic mixing [66]. Hence, the action for the gauge field is written as[2]

$$\mathcal{L}_{\rm gauge} \supset -\frac{1}{4}\hat{B}_{\mu\nu}\hat{B}^{\mu\nu} + \frac{\varepsilon}{2\cos\theta_W}\hat{B}_{\mu\nu}\hat{X}^{\mu\nu} - \frac{1}{4}\hat{X}_{\mu\nu}\hat{X}^{\mu\nu} - \frac{1}{2}(g_X\phi)^2\hat{X}_\mu\hat{X}^\mu, \tag{2.1}$$

where ε is a kinetic mixing, g_X is $\mathrm{U}(1)_{\rm dark}$ gauge coupling, and θ_W is the weak mixing angle. Due to the kinetic mixing, the kinetic terms of the gauge fields are not diagonal. They are diagonalized by some rotations among the gauge boson fields:

$$\mathcal{L}_{\rm gauge} \supset -\frac{1}{4}F_{\mu\nu}F^{\mu\nu} - \frac{1}{4}X_{\mu\nu}X^{\mu\nu} - \frac{1}{2}(\eta g_X\phi)^2 X_\mu X^\mu, \tag{2.2}$$

where $F_{\mu\nu}$ is electromagnetic field strength tensor, X_μ and $X_{\mu\nu}$ are diagonalized dark gauge boson field and its strength tensor and $\eta \equiv 1/\sqrt{1-\varepsilon^2/\cos^2\theta_W}$ (See appendix A for the detail.). Since ε is typically constrained by various experiments and observations, we always take it as a small parameter, and approximate $m_X \approx g_X\phi$. On this basis, X couples to the SM fermions, and such couplings are proportional to ε.

Although the photon is massless, it can obtain a non-zero effective mass through the interaction with particles in the thermal bath. For instance, Compton scattering with the electrons gives the real part of effective photon mass as [67, 68]

$$m_\gamma^2 = \begin{cases} 4\pi\alpha_{\rm em}(n_e/m_e) & \text{for} \quad T \ll m_e, \\ (2/3)\pi\alpha_{\rm em}T^2 & \text{for} \quad T \gg m_e, \end{cases} \tag{2.3}$$

where $\alpha_{\rm em} \approx 1/137$ is the fine structure constant and T is the temperature of the thermal bath. In the presence of the kinetic mixing, thermal effects also generate a non-diagonal mass term between the photon and dark gauge boson. In a basis where the photon and dark gauge boson mass terms are diagonal,[3] the effective kinetic mixing is given as [69]

$$|\bar{\varepsilon}(\omega,T)|^2 = \varepsilon^2\frac{m_X^4}{(m_X^2-m_\gamma^2)^2+(\omega D)^2}, \tag{2.4}$$

where ωD is the imaginary part of the effective photon mass [70].[4] This results in the kinetic mixing being suppressed in $m_X \ll m_\gamma$ limit, while there is a resonance at $m_X = m_\gamma$. In the resonance regime, the kinetic mixing is amplified as $|\bar{\varepsilon}| = \varepsilon m_X^2/(\omega D)$.

Let us now discuss the dynamics of the model. As shown in eq. (2.2), the mass of the dark gauge boson is proportional to the quintessence field value, which can be determined from its equation of motion [36],

$$\begin{aligned} \ddot{\phi} + 3H\dot{\phi} + \frac{\partial V_{\rm eff}(\phi)}{\partial\phi} &= 0, \\ V_{\rm eff}(\phi) = V_0(\phi) + \frac{1}{2}g_X^2 X_\mu X^\mu\phi^2, \end{aligned} \tag{2.5}$$

[2]The FLRW metric with $g_{\mu\nu} = (-1, a^2, a^2, a^2)$ is used.

[3]Due to the additional diagonalization, the mass of dark gauge boson in the medium and vacuum has a tiny difference proportional to ε, which we can neglect.

[4]$D \sim 8\pi\alpha_{\rm em}^2/(3m_e^2)n_e$ when $T \ll m_e$, and $\omega \sim T$.

JCAP03(2024)048

where $V_0(\phi)$ is the potential of ϕ, and $g_X^2 X_\mu X^\mu \phi^2/2$ is the gauge potential [36] which gives an additional contribution to the quintessence potential. While there is a freedom to choose $V_0(\phi)$ as long as it gives the required dark energy phenomenology,[5] we use the inverse-power potential suggested by Ratra and Peebles [4] throughout this paper:

$$V_0(\phi) = \frac{M^{\alpha+4}}{\phi^\alpha}, \tag{2.6}$$

where $\alpha > 0$, and M is chosen to fit the present-time dark energy density. In this work, we take $V_0(\phi)$ as a quantum effective potential, which includes all the quantum corrections.[6] This allows us to consider relatively larger g_X and m_X compared to our previous works [36, 37].[7]

The Ratra-Peebles potential has a tracking behavior, so the wide range of initial conditions eventually converge to one common tracking solution [71] given by [35]

$$\begin{aligned} \phi &\propto a^{3(1+w_b)/(2+\alpha)}, \\ \sqrt{\frac{\partial^2 V_0(\phi)}{\partial \phi^2}} &\sim 3H, \end{aligned} \tag{2.7}$$

where w_b is the equation-of-state parameter of the background component of the universe,[8] and the second line (which would be a quintessence field mass without the gauge potential) can be derived from eq. (2.5) with $X^\mu = 0$. However, the tracking solution of the ϕ field can be interrupted by the backreaction of the background dark gauge boson. If $V_{\rm eff}(\phi)$ is steep around the potential minimum such that $m_\phi = \sqrt{\partial^2 V_{\rm eff}/\partial\phi^2} \gg H$, ϕ field is trapped at the minimum of $V_{\rm eff}$ [37]. In this case, we approximate $\phi \sim \phi_{\rm min}$, where $\phi_{\rm min}$ is the value of ϕ at the potential minimum.

An explicit form of the backreaction can be computed from the thermal average of $\langle X_\mu X^\mu \rangle$ as [72]

$$\langle X_\mu X^\mu \rangle = 3 \int \frac{d^3\vec{p}}{(2\pi)^3} \frac{f(\vec{p})}{\sqrt{m_X^2 + |\vec{p}|^2}}, \tag{2.8}$$

where $f(\vec{p})$ is the phase space distribution of the dark gauge boson. This expression can be simplified if one assumes that the phase space distribution is isotropic and peaked at a certain momentum scale $|\vec{p}| \sim T$. If the dark gauge bosons are relativistic, $T \gg m_X$,

$$\langle X_\mu X^\mu \rangle \approx C \frac{n_X}{T}, \tag{2.9}$$

where n_X is the number density of the dark gauge boson, and C is the correction factor, which depends on the actual distribution. If the dark gauge boson follows the Bose-Einstein

[5] For the uncoupled quintessence field model, the dark energy phenomenology is obtained when $\sqrt{\partial^2 V_0/\partial\phi^2} \lesssim H$.

[6] Such corrections include vacuum energy of all field configurations and ϕ dependent correction from the dark gauge boson. We presume that there exists a UV theory that passes down the Ratra-Peebles potential as an IR effective potential regardless of the complication of the UV tree level potential.

[7] Possible constraints on g_X and m_X when taking the Ratra-Peebles potential as a tree-level potential are given in ref. [36].

[8] $w_b = 1/3$ for the radiation-dominated era, and $w_b = 0$ for the matter-dominated era.

JCAP03(2024)048

distribution, we found that $C = 0.68$. On the other hand, if the dark gauge bosons are non-relativistic, $T \ll m_X$, then

$$\langle X_\mu X^\mu \rangle \approx \frac{n_X}{m_X}. \tag{2.10}$$

Then, the condition for the trap of ϕ is written as

$$n_X \gg \begin{cases} \dfrac{H^2 T}{(\alpha+2) C g_X^2} & \text{for } T \gg m_X, \\ \dfrac{H^2 m_X}{(\alpha+2) g_X^2} & \text{for } T \ll m_X. \end{cases} \tag{2.11}$$

ϕ is easier to be trapped for a larger g_X. Also, this expression shows that even if ϕ is once trapped, it could be released to the tracking solution as n_X decays away or m_X increases.

One can also calculate $\phi_{\rm min}$ using eq. (2.9) or (2.10), then m_X is given as follows:

$$m_X \sim \begin{cases} \left(\dfrac{\alpha g_X^\alpha M^{4+\alpha}}{C \dfrac{n_X}{T}} \right)^{\frac{1}{\alpha+2}} & \text{for } T \gg m_X, \\ \left(\dfrac{\alpha g_X^\alpha M^{4+\alpha}}{n_X} \right)^{\frac{1}{\alpha+1}} & \text{for } T \ll m_X. \end{cases} \quad \text{(trapped)} \tag{2.12}$$

When the condition of eq. (2.11) is satisfied, we use eq. (2.12) to find m_X. In other case, we assume that ϕ follows the tracking solution, then m_X is given from the second line of eq. (2.7) as follows:

$$m_X \sim g_X \left(\frac{\sqrt{\alpha(\alpha+1)} M^{4+\alpha}}{3H} \right)^{\frac{2}{\alpha+2}}. \quad \text{(tracking)} \tag{2.13}$$

We presented a general formalism applicable to any values of $\alpha > 0$, and the following discussions are largely valid regardless of any $\alpha > 0$. In our quantitative analysis, including all figures, we will set $\alpha = 1$, for definiteness.

3 Production and decay of the dark gauge boson

The dark gauge boson can be produced from the SM thermal bath via kinetic mixing.[9] Since the effective kinetic mixing in the thermal bath largely depends on the mass of the dark gauge boson, it is crucial to incorporate a mass-varying effect in the production process. Also, the background dark gauge boson density can affect the evolution of the dark gauge boson mass, and we will demonstrate the self-consistent calculation of dark gauge boson density.

We investigate the production of a light dark gauge boson ($m_X \ll m_e$), which becomes heavier in the late universe due to the mass-varying nature.[10] For the light dark gauge boson,

[9] For an alternative production using the dark axion portal, see refs. [73, 74].

[10] If the dark gauge boson is heavier than $2m_e$, the dominant production channel is the pair coalescence ($e^+e^- \to X$) [70]. However, there is an upper limit to the production from this channel since sufficient background dark gauge boson would suppress m_X to be smaller than $2m_e$. (One can get the upper limit from eq. (2.12) by substituting $2m_e$ for m_X.) We checked that the contribution from the coalescence is negligibly small in the parameter space we consider in this paper.

JCAP03(2024)048

Compton-like process ($\gamma e^- \to X e^-$) is the dominant production channel [70]. Assuming that backreaction from X to SM thermal bath is negligible, or produced n_X is small compared to the SM thermal bath entropy density s, the Boltzmann equation is given as [75]

$$\frac{dn_X}{dt} + 3Hn_X = \frac{1}{2\pi^4}\int_{S_0}^{\infty} dS\; p_{12}^2\sqrt{S}\sigma_{\rm Comp}(S)\left(Te^{\mu/T}K_1\left(\frac{\sqrt{S}}{T}\right)\right), \tag{3.1}$$

where $S_0 = (m_e + m_\gamma)^2$, $p_{12} = \sqrt{S-(m_e+m_\gamma)^2}\sqrt{S-(m_e-m_\gamma)^2}/(2\sqrt{S})$, μ is the chemical potential of the electron, and T is the temperature of SM thermal bath. The effect of μ becomes significant below e^+e^- annihilation around $T \sim \mathcal{O}(10)\,\mathrm{keV}$ [76]. Also, $\sigma_{\rm Comp}$ is the Compton scattering cross-section given as [70]

$$\begin{aligned}\sigma_{\rm Comp}(S) = \frac{2\pi\alpha_{\rm em}^2\bar{\varepsilon}^2}{(S-m_e^2)^3}\Bigg(&\frac{\beta}{2S}(S^3 + 15S^2m_e^2 - Sm_e^4 + m_e^6 + m_X^2(7S^2 + 2Sm_e^2 - m_e^4)) \\ &+ 2(S^2 - 6Sm_e^2 - 2m_e^4 - 2m_X^2(S - m_e^2 - m_X^2))\log\left[\frac{S(1+\beta)+m_e^2-\mu^2}{2m_e\sqrt{S}}\right]\Bigg),\end{aligned} \tag{3.2}$$

where $S^2\beta^2 = (S-(m_e+m_X)^2)(S-(m_e-m_X)^2) \approx (S-m_e^2)^2$.

As discussed in ref. [70], the dark gauge boson is resonantly produced when $m_\gamma \approx m_X$. Since $m_X = g_X\phi$, the value of ϕ determines when the resonant production occurs. If there is no sufficient background density of X, then ϕ follows the tracking solution. We assume that the initial abundance of the dark gauge boson is negligibly small, and ϕ field initially follows the tracking solution, where the mass is given from eq. (2.13). If the sufficient dark gauge boson is produced before the resonance, the ϕ field follows the trapped solution, and its mass is given from eq. (2.12). For given parameters ε and g_X, we numerically solved the Boltzmann equation, eq. (3.1), with the tracking mass given in eq. (2.13) and checked whether a sufficient amount of X is produced for ϕ to be trapped. Once the trapping occurred, we checked when it happened, and from that time, we solved eq. (3.1) with the trapped mass in eq. (2.12). Based on this analysis, we can check the resonant behavior of the production.

The resonant behavior depends on whether ϕ is trapped or following the tracking solution when the resonance occurs. If ϕ follows the tracking solution, m_X monotonically increases over time, while m_γ decreases over time. So, there is an instantaneous moment when m_X and m_γ coincide, and the resonance occurs in an instant. In the case of the trapped ϕ, however, the resonant production of X suppresses m_X [eq. (2.12)]. If the production is sufficiently large to keep m_X from surpassing m_γ, then m_X could follow m_γ during some period. Therefore, the resonance can be sustained until the production rate becomes too weak due to the dilution of the photon and electron by the expansion of the universe. Figure 1 shows examples of the production for each case. The blue (cyan) curve corresponds to the trapped (tracking) case, respectively. In figure 1(a), the number density of X normalized by the SM thermal bath entropy density s ($Y_X \equiv n_X/s$), drastically increases at the resonance, i.e. when $m_X = m_\gamma$ holds. Also, figure 1(b) shows that m_X of the trapped case (blue curve) follows m_γ (red curve) during some interval. This extended resonance clearly enhances Y_X by several orders of magnitude compared to the tracking case.

The resultant Y_X, for each ε and g_X, when X is produced is given in figure 2(a). The parameter space below the blue curve corresponds to the tracking production, and the other

JCAP03(2024)048

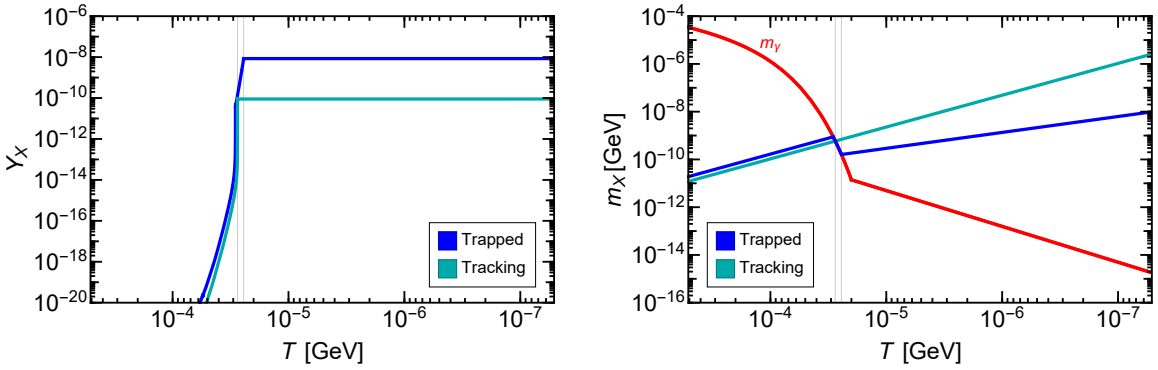

(a) Y_X. (b) m_X and m_γ.

Figure 1. Examples of the evolution of $Y_X \equiv n_X/s$ and m_X around resonant production. The blue curve corresponds to the trapped production ($g_X = 5 \times 10^{-19}$). The cyan curve corresponds to the tracking production ($g_X = 3 \times 10^{-19}$). Both scenarios share $\varepsilon = 10^{-11}$ in common. The thin vertical lines correspond to when the resonant production finishes. The red curve in (b) corresponds to the effective photon mass. The production of the trapped case is much larger compared to the tracking case because the resonance period is extended. (We set $\alpha = 1$ throughout this work.)

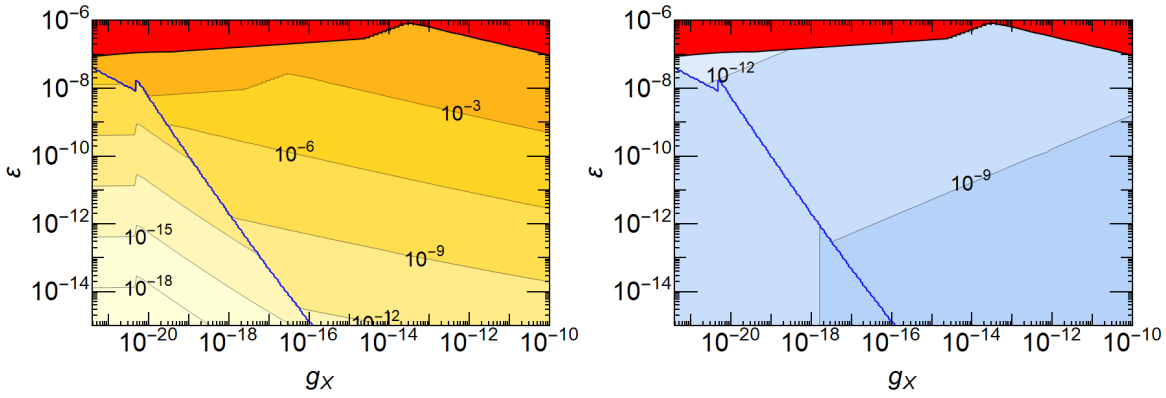

(a) Y_X. (b) m_X [GeV].

Figure 2. The dark gauge boson density normalized by the entropy density of SM thermal bath ($Y_X \equiv n_X/s$) and the mass (m_X) when they are resonantly produced. The red region corresponds to the parameter space that gives $Y_X \geq 1$. The blue curve is the boundary between the tracking (below) and trapped (above) cases.

side corresponds to the trapped production. The production of X is amplified in the trapped case, as the resonance is extended. Also, figure 2(b) shows the mass of the dark gauge boson when it is produced. Both the density and mass of the dark gauge boson change significantly across the blue curve. The contour lines below the blue curve in figure 2(b) are vertical since the tracking solution does not depend on Y_X (n_X) [eq. (2.13)].

After the resonant production, there are two scenarios for the dark gauge bosons, depending on whether they (i) decay into other components, or (ii) remain as the sub-dominant mass-varying dark matter. The main decay channels of the dark gauge boson are

JCAP03(2024)048

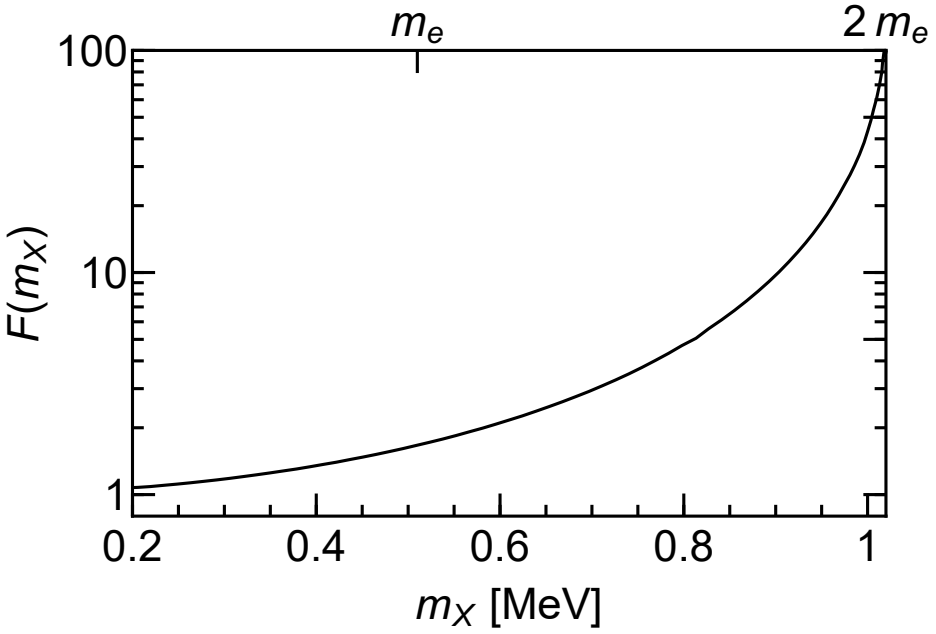

Figure 3. Enhancement factor $F(m_X)$ for three-photon decays. Reproduced from [79]. CC BY 4.0.

$X \to \gamma\gamma\gamma$,[11] and $X \to e^+e^-$ processes. The decay products (three photons, and e^+e^- pair) might become the main signal of the gauged quintessence model.

Figure 2(b) shows that initially, the mass of the dark gauge boson was smaller than $2m_e$ in the parameter space of interest. Therefore, in the early universe, the $X \to e^+e^-$ channel is closed, but the $X \to \gamma\gamma\gamma$ process can occur. $X \to \gamma\gamma\gamma$ decay rate below e^+e^- threshold ($m_X < 2m_e$) is given by [78, 79]

$$\Gamma_{\gamma\gamma\gamma} = F(m_X)\frac{17\alpha_{\rm em}^4\bar{\varepsilon}^2}{11664000\pi^3}\frac{m_X^9}{m_e^8}, \tag{3.3}$$

where $F(m_X)$ is the enhancement factor, which leads to a substantial effect when m_X is close to $2m_e$. $F(m_X)$ is described in figure 3 [79]. If $\Gamma_{\gamma\gamma\gamma}$ becomes larger than Hubble parameter H, most of the dark gauge boson energy density is converted to the photon energy density.

As the mass of the dark gauge boson grows according to either eq. (2.12) or eq. (2.13), $X \to e^+e^-$ channel can open when the mass of the dark gauge boson crosses e^+e^- threshold. e^+e^- decay rate is given by

$$\Gamma_{e^+e^-} = \frac{\alpha_{\rm em}\bar{\varepsilon}^2 m_X}{3}\sqrt{1-\left(\frac{2m_e}{m_X}\right)^2}\left(1+\frac{2m_e^2}{m_X^2}\right). \tag{3.4}$$

If $X \to \gamma\gamma\gamma$ process does not deplete the dark gauge boson before m_X reaches the threshold $2m_e$, then the remaining dark gauge bosons can decay into e^+e^- pairs. This is one of the

[11]The dark gauge bosons also decay to neutrinos ($X \to \nu\bar{\nu}$), and this is the dominant decay channel if the dark gauge boson is lighter than $\mathcal{O}(10)$ keV [77]. However, X density is hardly affected by the neutrino decay even when the neutrino channel is the dominant one, since the decay rate into the neutrinos is extremely small. For instance, with the most promising set of parameter $\varepsilon = 10^{-7}$ and $m_X = 10\,\text{keV}$, one obtains $\Gamma_{\nu\bar{\nu}}/H_0 \sim 10^{-10}$.

JCAP03(2024)048

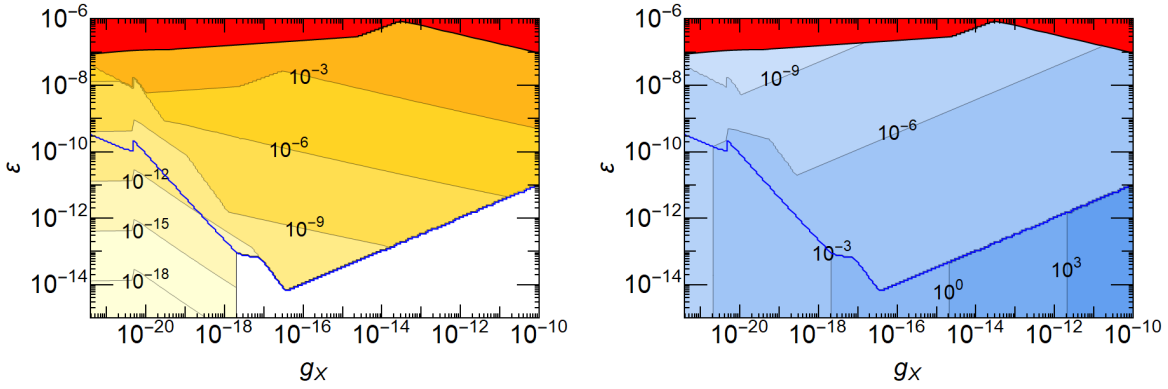

(a) Y_X at $T = T_{\rm eq}$.

(b) m_X [GeV] at $T = T_{\rm eq}$.

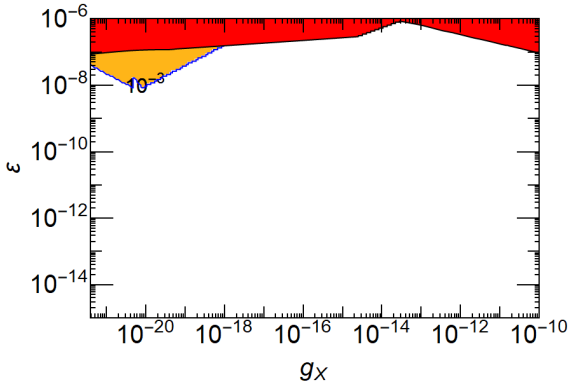

(c) Y_X at $T = T_0$.

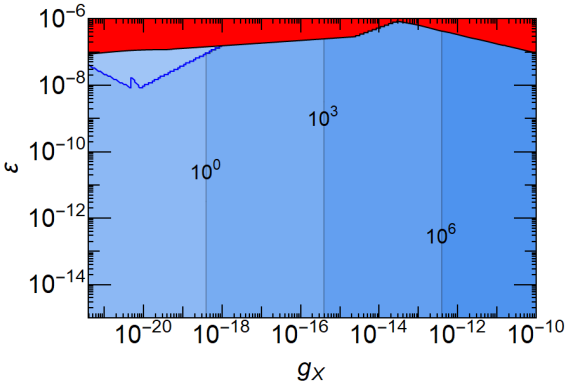

(d) m_X [GeV] at $T = T_0$.

Figure 4. Time evolution of n_X/s and m_X. Each figure corresponds to n_X/s or m_X at (a, b): $T = T_{\rm eq}$, (c, d): $T = T_0$. The blue curve corresponds to the boundary between tracking (below) and trapped (above) cases at each moment. The blank region indicates that X has decayed into other components before reaching the specified time.

unique features of our model. Since the three-photon decay is strongest near e^+e^- threshold [eq. (3.3)], we expect most of the photons from $X \to \gamma\gamma\gamma$ are produced right before the beginning of the generation of e^+e^- signal.

The time evolution of Y_X and m_X are described in figure 4. As time goes by, the decay rate becomes larger than the Hubble parameter, and the decay of the dark gauge boson happens in some parameter space. The parameter space where decays happen before $T = T_{\rm eq}$ and $T = T_0$ is described as the blank region in figure 4(a) and figure 4(c). If X decays into other components, then n_X becomes negligible, and m_X follows the tracking solution so the contour lines below the blue curve in figure 4(b) and figure 4(d) become vertical.

In the parameter space beyond the left border of figure 4, X can remain as a remnant until the present. In this case, the dark gauge bosons exist as mass-varying dark matter in the universe.

JCAP03(2024)048

4 Constraints

Various studies have investigated the constraints on the U(1) gauge extension of the standard model. Many of these constraints are relevant to our scenario. However, due to the mass-varying effect, the shape of constraints is quantitatively and qualitatively different. We will discuss the constraints on our model from over-production, CMB spectrum distortion and diffuse X-ray/gamma-ray background. Figure 5 summarizes these constraints. ϕ follows the tracking solution in the remaining parameter space. In this case, the present mass of dark gauge boson (m_X^0) is given as $3 \times 10^{18}\ g_X\,\mathrm{GeV}$, corresponding to the labels in the upper boundary.

4.1 Overproduction

If the extra energy density dominates the total energy density of the universe, it can modify the background expansion of the universe. This affects the theoretical estimation of BBN, CMB, and galaxy distributions.

Since the production of the dark gauge boson mainly occurs after the BBN, our scenario is not constrained by the BBN. However, the production of the dark gauge boson reduces the energy density and number density of the photon. Since the neutrinos are unaffected by the production of the dark gauge boson, this leads to the increase of the effective number of the neutrino (N_ν^{eff}) as [80]

$$N_\nu^{\mathrm{eff}} \equiv \frac{\rho_{\mathrm{rad}} - \rho_\gamma}{\rho_\nu^{\mathrm{SM}}} = \frac{3.046}{1-x}, \tag{4.1}$$

where $0 \leq x < 1$ is the fraction of the dark gauge boson density to the photon density right after the resonant production; ρ_{rad}, ρ_γ, and ρ_ν^{SM} is the energy density of the total radiation degree of freedom, photon, and neutrino, respectively.[12] *Planck* TT,TE,EE+lowE gives a constraint on this quantity as $N_\nu^{\mathrm{eff}} = 2.92^{+0.36}_{-0.37}$ [34]. We give a constraint from N_ν^{eff} by the brown region in figure 5.

An additional radiation or matter density can change the time of the matter-radiation equality. *Planck* [34] also constrains the redshift at the matter-radiation equality as $z_{\mathrm{eq}} = 3402 \pm 26$. In the absence of the additional density, the scale factor[13] at the equality ($\bar{a}_{\mathrm{eq}}$) is

$$\rho_{\mathrm{m}}^0 \bar{a}_{\mathrm{eq}}^{-3} = \rho_{\mathrm{rad}}^0 \bar{a}_{\mathrm{eq}}^{-4}, \tag{4.2}$$

where ρ_{m}^0 (ρ_{rad}^0) is the present energy density of matter (radiation). Then, the matter-radiation equality is shifted by the dark gauge boson density as

$$\rho_{\mathrm{m}}^0 {a_{\mathrm{eq}}}^{-3} \pm \rho_X(a_{\mathrm{eq}}) = \rho_{\mathrm{rad}}^0 {a_{\mathrm{eq}}}^{-4}, \tag{4.3}$$

where the plus (minus) sign is applied when X is non-relativistic (relativistic), respectively, and $\rho_X(a_{\mathrm{eq}})$ is the energy density of X at a_{eq}. Then we can find the following relation

[12] If the dark gauge boson is relativistic around the CMB decoupling, there is a dark gauge boson contribution to N_ν^{eff} [80]. However, this contribution is negligible unless $x > \mathcal{O}(0.1)$. Since the constraint obtained from N_ν^{eff} by considering the sole neutrino contribution is much stronger, one can ignore this contribution.

[13] The scale factor (a) and the redshift (z) are related as $a = 1/(z+1)$.

JCAP03(2024)048

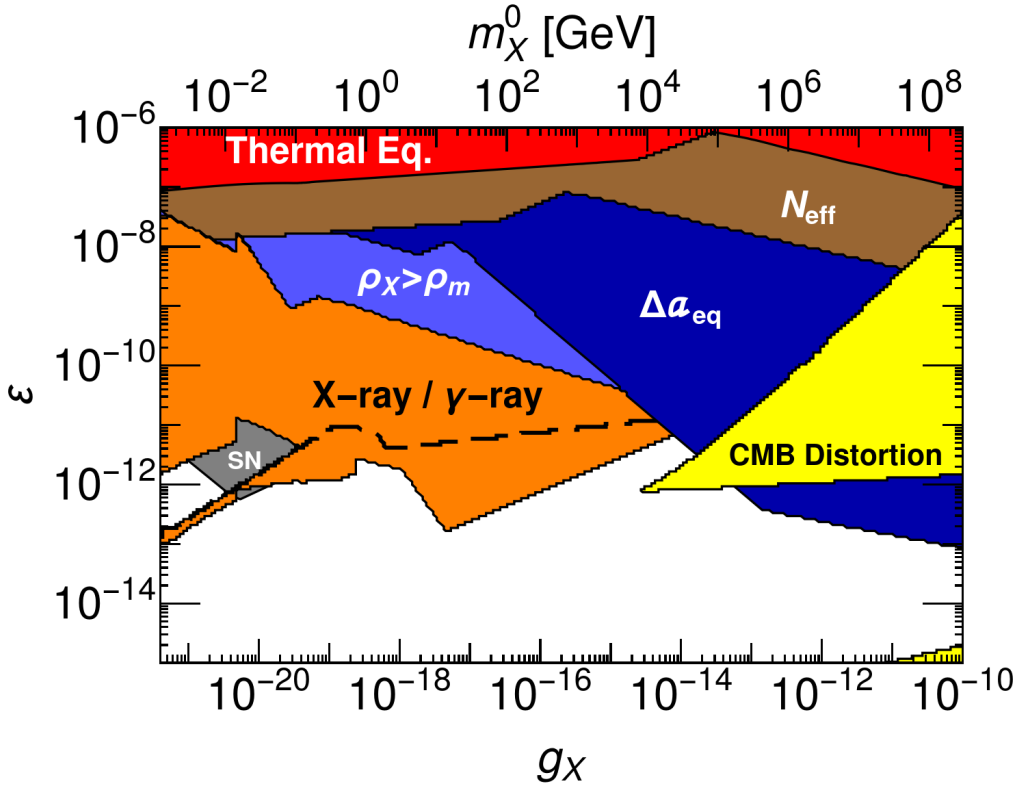

Figure 5. Constraints on ε and g_X when the dark gauge boson mass varies over time. The present mass of dark gauge boson (m_X^0) is given as $3 \times 10^{18}\ g_X$ GeV. The brown region is constrained by the change of $N_\nu^{\rm eff}$ after the resonant production. The deep blue (light blue) region is constrained by the over-density at the matter-radiation equality (during the matter-dominated era). The gray region corresponds to the constraint from supernova [81–83]. The CMB spectrum distortion constrains the yellow region, and the diffuse X-ray/gamma-ray background spectrum constrains the orange region. The small island of CMB constraint at the lower-right corner emerges due to the considerable amount of kinetic energy of e^+ and e^- from X decay, while the produced e^+ and e^- are non-relativistic in the other region of the parameter space. Above the dashed line, the dark gauge bosons are depleted before their mass crosses the e^+e^- threshold. Although we do not represent in this plot, the weak gravity conjecture [84] disfavors too tiny gauge coupling as $g_X \lesssim m_\phi/M_{\rm Pl} \sim 10^{-61}$. (Also, the inflationary scenario might be restricted [85, 86].) A kinetic mixing might originate from the fields that are charged under both the SM U(1) gauge symmetry and $\mathrm{U}(1)_{\rm dark}$ [66]. In this case, the kinetic mixing is estimated as $\varepsilon \sim 10^{-2} g_X$. Moreover, an even smaller kinetic mixing such as $\varepsilon \sim 10^{-13} g_X$ might be generated by the graviton-mediated interaction alone [87].

from 2 σ uncertainty of $z_{\rm eq}$ as

$$\left|\frac{\Delta a_{\rm eq}}{a_{\rm eq}}\right| \approx \frac{\rho_X(\bar{a}_{\rm eq})}{\rho_m^0 \bar{a}_{\rm eq}^{-3}} < \frac{52}{3403}, \tag{4.4}$$

where $\Delta a_{\rm eq} = a_{\rm eq} - \bar{a}_{\rm eq}$ is the shift of the matter-radiation equality. The constraint from the equality is described by the deep blue region in figure 5.

JCAP03(2024)048

After the dark gauge boson becomes non-relativistic, some fraction of the dark gauge boson density over the matter density would grow due to the increasing mass. If the energy density of the dark gauge boson is comparable to or surpasses the matter density, it affects the growth of the matter density fluctuation and the lensing of the CMB photons. A detailed analysis is required to verify the actual constraints, and we will leave it to future works. Instead, we mark the light blue region in figure 5, where $\rho_X/\rho_m > 1$ is achieved after the matter-radiation equality.[14]

4.2 CMB spectrum distortion

In the early universe, CMB photons obtain the blackbody spectrum from processes such as Compton scattering, double Compton scattering, and Bremsstrahlung. However, these processes become inefficient as the universe cools down. For instance, if the temperature of the SM thermal bath drops below $T \sim 100$ eV, double Compton scattering and Bremsstrahlung processes are not effective in producing high energy photons, which leads to the loss of the chemical equilibrium. Also, the kinetic equilibrium is broken when the Compton scattering becomes inefficient from $T \sim 10$ eV. Therefore, the energy injection to the SM thermal bath below $T \sim 100$ eV can cause the distortion of the CMB spectrum [88].

Such a CMB spectrum distortion is highly constrained by COBE/FIRAS [89] as $|\mu| < 4.7\times 10^{-5}$ and $|y| < 1.5 \times 10^{-5}$ [90]. μ-type distortion is mostly generated by the energy injection between the decoupling of the double Compton scattering and the Compton scattering, while y-type distortion is generated after the decoupling of the Compton scattering.

When $m_X \leq 2m_e$, the dark gauge boson deposits its energy and entropy density by the three-photon decay process. In this case, μ and y-type distortions from the Green's function formalism are given by [91–94]

$$\mu \approx 1.401 \int \frac{\mathcal{J}_{bb}(T)\,(1-\mathcal{J}_y(T))}{\rho_\gamma(T)} \left(\frac{1}{\rho_\gamma(T)} \frac{d\rho(T)}{dT} - \frac{4}{3n_\gamma(T)} \frac{dn(T)}{dT} \right) dT, \tag{4.5}$$

$$y \approx \frac{1}{4} \int \frac{\mathcal{J}_y(T)}{\rho_\gamma(T)} \frac{d\rho(T)}{dT} dT, \tag{4.6}$$

where $d\rho(T)/dT$ is the power injected to the SM thermal bath, $dn(T)/dT$ is the rate of the photon entropy (number density) injection, $\rho_\gamma(T)$, $n_\gamma(T)$ are the energy density, number density of CMB photons, and $\mathcal{J}_{bb}(T)$, $\mathcal{J}_y(T)$ are numerically evaluated Green's functions given by [94]

$$\mathcal{J}_{bb}(z) = \exp\left[-\left(\frac{T}{T_\mu} \right)^{5/2} \right], \tag{4.7}$$

$$\mathcal{J}_y(z) = \begin{cases} \left(1 + \left(\frac{T}{T_y} \right)^{2.58} \right)^{-1} & \text{for } T > T_{\rm eq}, \\ 0 & \text{for } T < T_{\rm eq}, \end{cases} \tag{4.8}$$

[14] If the resonant production occurs after $T \sim 100\,\text{eV}$, there might be a distortion from the resonance. However, for the parameter space of interest, the resonant production occurs when $T \gg 100\,\text{eV}$, and we can neglect the distortion from the resonance.

JCAP03(2024)048

where $T_\mu = 460\,\mathrm{eV}$ and $T_y = 13.9\,\mathrm{eV}$. Also, the injected power can be calculated from the following equation,

$$\frac{d\rho}{dt} \sim \Gamma_{\gamma\gamma\gamma} m_X(T) n_X(T), \tag{4.9}$$

and $d\rho/dt = TH(T)d\rho/dT$ from the chain rule. $n_X(T)$ can be calculated from the Boltzmann equation, so the injected power can be written as

$$\frac{d\rho}{dt} \sim \Gamma_{\gamma\gamma\gamma} m_X(T) \exp\left[-\frac{\Gamma_{\gamma\gamma\gamma}}{\eta H}\right] \left(\frac{2\pi^2}{45} g_{*s} T^3\right) Y_X, \tag{4.10}$$

where $g_{*s} \approx 3.9$ is the effective degrees of freedom of SM thermal bath entropy density. The exponential factor describes the change of n_X due to the decay, and η is the correction due to the mass-varying nature of the dark gauge boson. (See appendix B for the detail.)

If the dark gauge boson is not depleted before its mass reaches $2m_e$, the remaining dark gauge bosons decay into e^+e^- pairs. Since electrons and baryons maintain full thermal contact with photons until $T \sim 50$ meV, the thermal energy (kinetic energy) of e^+ and e^- quickly kinetically equilibriate, leading to the CMB distortion through the energy injection term in eqs. (4.5) and (4.6). As we will demonstrate in section 5, $X \to e^+e^-$ decay occurs in a short period near e^+e^- threshold. Thus, we approximate the decays occur mostly at T_{dec}, where $\Gamma_{e^+e^-}(T_{\mathrm{dec}}) = H(T_{\mathrm{dec}})$, and the kinetic energy of a single e^+ or e^- is given by

$$E_k \sim \frac{1}{2m_e}\left(\frac{1}{4} m_X^2(T_{\mathrm{dec}}) - m_e^2\right). \tag{4.11}$$

Consequently, the energy injected into the CMB photons is expressed as

$$\Delta\rho \sim \Delta n_{e^+e^-}(E_k - \frac{3}{2} T_{\mathrm{dec}}), \tag{4.12}$$

where $\Delta n_{e^+e^-}$ represents the number density of e^+ and e^- released by $X \to e^+e^-$ decays.

The constraint from the CMB spectrum distortion is represented by the yellow region in figure 5. Since e^+ and e^- generated from the dark gauge boson decay are non-relativistic, this constraint mostly arises from the $X \to \gamma\gamma\gamma$ processes. One exception arises at the lower-right corner of figure 5. In this regime, e^+e^- decay occurs when m_X is on the order of a few MeV, leading to the production of e^+ and e^- with substantial kinetic energy. In contrast to the common idea that the stronger coupling gives a stronger constraint, the CMB spectrum distortion does not constrain the large ε regime. This is because the larger ε leads to the larger dark gauge boson density, which suppresses the mass of the dark gauge boson (see figure 4(b)). Thus the three-photon decay is not efficient [eq. (3.3)] in the early universe.

4.3 Diffuse X-ray/gamma-ray

The photon produced by the decay of the dark gauge boson constitutes an isotropic diffuse photon background. Such a diffuse X-ray/gamma-ray background spectrum was measured by various missions in the frequency window between 1 keV to 10 GeV [95–101]. Therefore, $X \to \gamma\gamma\gamma$ signal in this frequency band can give a significant constraint.

JCAP03(2024)048

The X-ray/gamma-ray flux from the decay of the dark gauge boson is given by [102–107]

$$\frac{d^2\Phi_\gamma}{d\Omega dE} = \frac{3}{4\pi}\int \frac{dN}{dE(z)}\frac{n_X(z)}{(1+z)^3}\frac{\Gamma_{\gamma\gamma\gamma}(z)}{H(z)}dz, \tag{4.13}$$

where $dN/dE(z)$ is the spectrum of the photon from the dark gauge boson decay at the redshift z, and $E(z) = E_0(1+z)$ is the energy of the photon at z which is detected with the energy E_0. If one assumes the typical monochromatic decay[15] [70, 108], i.e. $dN/dE(z) = \delta(E(z) - m_X/3)$, the simplified formula is given by

$$\frac{d^2\Phi_\gamma}{d\Omega dE} = \frac{3}{4\pi}\frac{\Gamma_{\gamma\gamma\gamma}(z^*)n_X(z^*)}{E_0 H(z^*)(1+z^*)^3}, \tag{4.14}$$

where z^* is the redshift which satisfying $E(z^*) = m_X(z^*)/3$. Unlike the conventional decaying dark matter models[16] where the mass of the particles is fixed, the slope of the measured flux is affected by the time-variation of $\Gamma_{\gamma\gamma\gamma}$. We take that the three-photon decay terminates when m_X crosses e^+e^- threshold or the three-photon decay rate becomes larger than the Hubble parameter. The constraint from the diffuse X-ray/gamma-ray from the collection of data in ref. [100] is given by the orange region in figure 5. The orange region above the dashed line is where the dark gauge bosons are depleted before m_X crosses the e^+e^- threshold. In this regime, the overall magnitude of the signal is weaker because the decay occurs below the e^+e^- threshold [eq. (3.3)]. On the other hand, below the dashed line, the dark gauge bosons are not depleted before they reach the e^+e^- threshold. Therefore, the decay mostly happens near the threshold where the decay rate is maximal. This is why the constraint appears in the small ε region, while some of the larger ε parameter space is not constrained.

5 Dark energy signal

So far, we have discussed how dark energy can affect the production and decay of dark gauge bosons. In this section, we will explore how the effects of dark energy can manifest in distinct non-gravitational signals.

As we mentioned, the dark gauge boson can decay into three photons or e^+e^- pair. In the case of the conventional dark photon model, the decay of the gauge boson can either produce e^+/e^- signal or three photon signal depending on its mass, but it cannot have both signals simultaneously [70]. In our scenario, however, the increasing mass of the dark gauge boson due to the rolling of the quintessence field dark energy field allows the dark gauge boson to decay into three photons when the mass of the dark gauge boson is smaller than $2m_e$, and it decays to e^+e^- pair as the mass of dark gauge boson becomes larger than $2m_e$. Therefore, both signals can be produced together. This is demonstrated in figure 6 which shows the present energy density of decay products $\rho^0_{\gamma\gamma\gamma}$ and $\rho^0_{e^+e^-}$ normalized by the critical density $\rho_{\rm crit} \simeq 3\times10^{-47}\,{\rm GeV}^4$. The left border of the figure 6 represents the kinematic threshold, beyond which the production of e^+/e^- signal is not possible, because

[15] An inclusion of actual decay spectrum can alter the flux [107]. However, the one-photon spectrum is mostly distributed around $E(z) \sim m_X/3$ [78], so the monochromatic decay approximation is valid.

[16] We classify conventional decaying dark matter models as those where the couplings and masses of particles involved in the decay processes are fixed, and the mother particles are non-relativistic.

JCAP03(2024)048

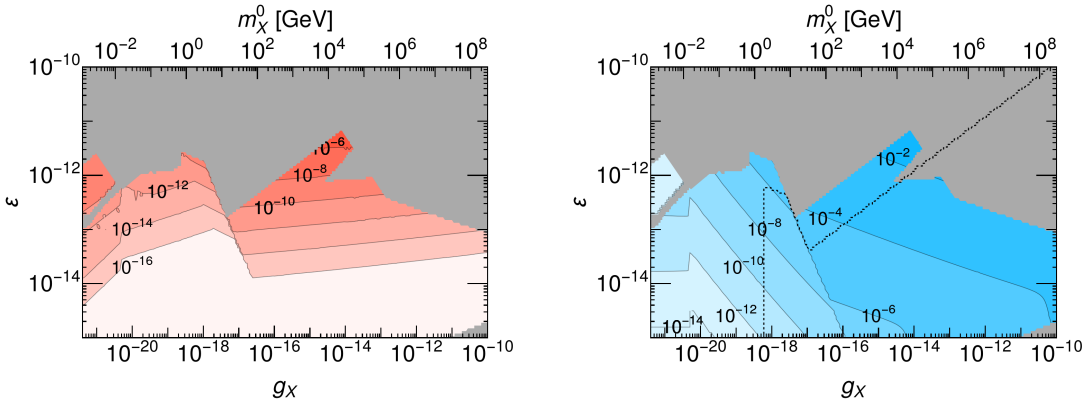

(a) $\rho^0_{\gamma\gamma\gamma}/\rho_{\rm crit}$. (b) $\rho^0_{e^+e^-}/\rho_{\rm crit}$.

Figure 6. The present energy density of the photon signal (red contours) and e^+/e^- signal (blue contours) produced by the dark gauge boson decay. The present mass of the dark gauge boson (m_X^0) is given as 3×10^{18} g_X GeV. Both energy densities are normalized by the critical density $\rho_{\rm crit} \simeq 3 \times 10^{-47}\,{\rm GeV}^4$. The gray region represents the collection of the constraints in figure 5. We do not show the contours below the $\rho^0/\rho_{\rm crit} = 10^{-16}$. Above the dotted curve, e^+/e^- signal is produced after the recombination ($z \sim 1100$).

the mass of the dark gauge boson is below the kinematic threshold. Except for the small region on the left corner surrounded by the gray constraint, both e^+/e^- and three photon signal can be produced together.[17]

The existing constraint from diffuse X-ray/gamma-ray overlaps with the region where e^+/e^- density could be produced. This suggests that future technical advancements may enable the exploration of photonic channels toward the unconstrained parameter space. If e^+/e^- signals can be probed as well, it would lead to an interesting discovery. Cosmic ray e^+/e^- spectrum has been widely observed by various missions such as PAMELA [109], Fermi-LAT [110], AMS [111], HESS [112], DAMPE [113], and CALET [114]. Although our e^+/e^- signals are highly non-relativistic, they could be accelerated by the strong magnetic field [115] and contribute as an excess e^+/e^- signal. Also, they might leave observable imprints through the scattering with baryons or high energy cosmic rays. We also note that e^+/e^- signal can be generated after the recombination, above the dotted line in figure 6, while conventional dark photon model with $\varepsilon > 10^{-15}$ cannot produce the background e^+/e^- signal after the recombination ($z \sim 1100$).

Figure 7 is the schematic description of the production and decay of the dark gauge boson. Normalized production/decay rate of each species (dY_i/dt, where Y_i is the normalized energy density of each species $i = \{X, \nu, \gamma, e\}$) shows the chronological order of each event. Since the three-photon decay rate has a steep dependence on m_X ($\Gamma_{\gamma\gamma\gamma} \propto m_X^9$), most of the three-photon decay might happen near e^+e^- threshold. The produced energy density of the photon signal is calculated by solving the Boltzmann equation. If m_X crosses the threshold before the dark gauge bosons are depleted, the remaining dark gauge bosons can

[17] In this region, the dark gauge bosons deplete before they cross the e^+e^- threshold.

JCAP03(2024)048

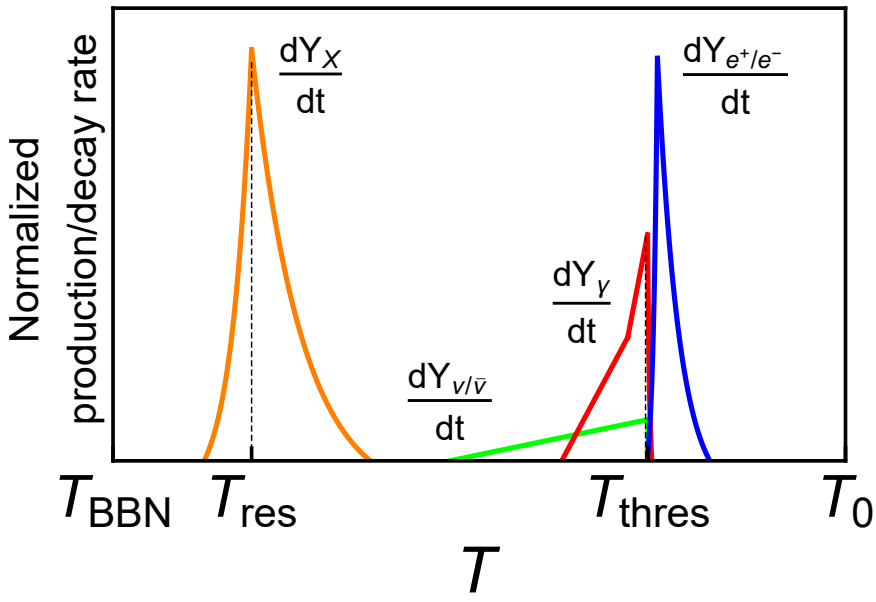

Figure 7. A schematic description of the production and decay of the dark gauge boson. Y_i denotes the normalized number density of each particle species $i = \{X, \nu, \gamma, e\}$. The orange curve is the normalized production rate of the dark gauge boson: dY_X/dt, and each of red, blue, green curve is the production rate of the photon: dY_γ/dt, positron/electron: $dY_{e^+/e^-}/dt$, neutrino/anti-neutrino: $dY_{\nu/\bar{\nu}}/dt$ from the decay of the dark gauge boson. The dark gauge bosons are resonantly produced at $T_{\rm res}$, and productions of the photon, neutrino and e^+/e^- signals mostly occur near e^+e^- threshold $T_{\rm thres}$ when $m_X \sim 2m_e$ is achieved.

decay into e^+e^- pairs. Interestingly, we found that the remaining dark gauge bosons almost instantaneously decay to e^+e^- pairs, i.e. $\Gamma_{e^+e^-} > H$, near e^+e^- threshold. This is because the $X \to e^+e^-$ process is blocked, resembling water contained behind a sealed dam, until the kinematic threshold is surpassed.[18] Therefore, the remaining dark gauge boson energy density is quickly converted to the e^+e^- pair energy density. Also, the produced e^+ and e^- are non-relativistic since they are produced right at the threshold. It could be the signal from the gauged dark energy model if one can observe the exotic photonic and e^+/e^- signal together.

Also, the gauged quintessence model can have a unique diffuse X-ray/gamma-ray spectrum. Figure 8 shows the spectrum of the photon arising from the decaying particles both from the gauged quintessence model and the conventional decaying dark matter models. In the conventional model, the overall X-ray/gamma-ray signal from n-body process is proportional to the decay rate ($\Gamma_{\rm dm}$), number density of the dark matter particle ($n_{\rm dm}$), and mass of the dark matter ($m_{\rm dm}$). If one assumes the monochromatic decay, then the decay signal is peaked at $m_{\rm dm}/n$, and the measured flux is proportional to $\sqrt{E/E_{\rm peak}}/\sqrt{1+3(E/E_{\rm peak})^3}$. Therefore, the slope of the measured X-ray/gamma-ray spectrum is universal regardless of the detail of the model.

However, the diffuse X-ray/gamma-ray spectrum in the gauged quintessence model could be completely different from the conventional model. Since the decay rate is proportional

[18] An exception appears only at the small portion of the bottom right corner of figure 6. However, even in this region, the decay occurs when m_X and the energy of resultant e^+e^- are a few MeV.

JCAP03(2024)048

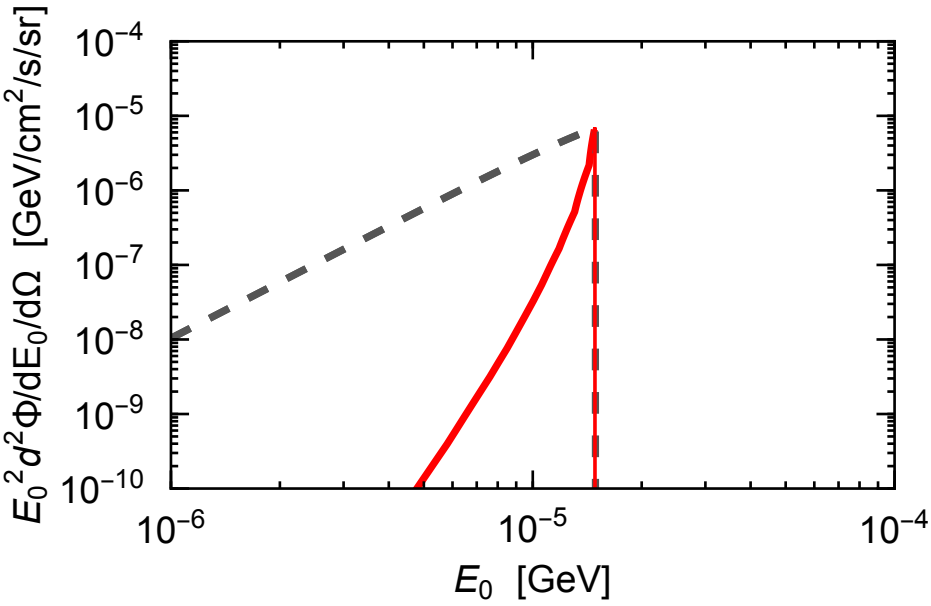

Figure 8. The diffuse X-ray/gamma-ray spectrum from the gauged quintessence (red) and conventional decaying dark matter model (dashed gray). The red curve represents the actual spectrum with $\alpha = 1$, $g_X = 10^{-20}$, $\varepsilon = 6.3 \times 10^{-13}$, while the gray curve is rescaled to give the same peak energy and peak signal magnitude to the red curve. For any conventional decaying dark matter model, regardless of the mass of the decaying particle or the decay rate, the slope of the gray curve is proportional to $(E/E_{\rm peak})^{5/2}/\sqrt{1+3(E/E_{\rm peak})^3}$, where $E_{\rm peak}$ is the peak energy [106]. The red curve is steeper because $\Gamma_{\gamma\gamma\gamma}$ has a sharp dependence on m_X.

to very large powers of m_X ($\Gamma_{\gamma\gamma\gamma} \propto m_X^9$), the decay rate rapidly grows with increasing m_X. This results in the higher energy part of the diffuse photon spectrum, generated in a more recent era, being amplified compared to the lower energy part of the spectrum. Therefore, the spectrum's slope becomes much steeper than the conventional decaying dark matter model.

Before closing this section, we briefly comment on the neutrino signal in our scenario. Neutrinos can also be produced by $X \to \nu\bar{\nu}$ process. Generated neutrino flux can be calculated from eq. (4.14) by replacing $3\Gamma_{\gamma\gamma\gamma}$ to $2\Gamma_{\nu\bar{\nu}}$. Similar to the three-photon decay rate, $\Gamma_{\nu\bar{\nu}}$ also grows with increasing m_X ($\Gamma_{\nu\bar{\nu}} \propto m_X^5$). Therefore, the diffuse neutrino spectrum also becomes sharper by the mass-varying effect. Although the neutrino decay spectrum is too small to be detected by current observations,[19] they remain as the potentially interesting observational window.

6 Summary and conclusion

In this work, we investigated non-gravitational signals from the gauged dark energy sector with a realization in the gauged quintessence model. The dark sector (quintessence field scalar + dark gauge boson) is connected to the SM sector via portals, and we studied the vector portal case. The time-varying dark energy field makes the mass of the dark gauge boson

[19]The neutrino decay rate may be enhanced if the dark gauge boson has an additional mass mixing [116–118].

JCAP03(2024)048

evolve during cosmic history. Since the production and decay of the dark gauge boson are deeply related to its mass, this makes the phenomenology of the dark gauge boson completely different from the conventional dark photon model of the same vector portal. For instance, the large number density of the dark gauge boson can backreact to the dynamics of the quintessence field dark energy. This makes the resonance production of the dark gauge boson in the thermal plasma enhanced through the extended resonance stage.

One of the interesting features of our scenario is that the decay channel of the dark gauge boson to the electron-positron pair might be closed in the early universe because the mass of the dark gauge boson was below e^+e^- kinematic threshold. So, the dark gauge boson decays to the three-photon and neutrinos in the early universe, but the remaining dark photon is converted to e^+e^- pair when the mass of the dark gauge boson crosses e^+e^- threshold. Therefore, we may have the exotic relic photons, neutrinos, and e^+e^- together. If the exotic relic photons/neutrinos produced by the decay of the dark gauge boson contribute to the diffuse photon/neutrino background, its spectrum could be distinguished from the conventional decaying dark matter signal. We also expect e^+/e^- might give the excess cosmic e^+/e^- flux, or produce secondary signals by the scattering with baryons or high energy cosmic rays.

So far, the research on dark energy phenomenology has mainly focused on the gravitational effect of dark energy through the modification of the universe's expansion near the present. Through this work, we emphasize that dark energy can significantly affect other sectors of the universe by non-gravitational interaction based on the gauge principle, and we might be able to explore the physics of dark energy with those signals.

Acknowledgments

We thank Daniel Chung for the helpful discussions. This work was supported in part by the JSPS KAKENHI (Grant No. 20H00160) and the National Research Foundation of Korea (Grant No. NRF-2021R1A2C2009718).

A Diagonalization of kinetic and mass terms

The kinetic terms for the Abelian gauge fields can be diagonalized by the following rotation of the fields as

$$\begin{bmatrix} \hat{B}_\mu \\ \hat{X}_\mu \end{bmatrix} = \begin{bmatrix} 1 & \eta\frac{\varepsilon}{c_W} \\ 0 & \eta \end{bmatrix} \begin{bmatrix} \tilde{B}_\mu \\ \tilde{X}_\mu \end{bmatrix}, \tag{A.1}$$

where $c_W \equiv \cos\theta_W$, $\eta = 1/\sqrt{1-\varepsilon^2/c_W^2}$. Then, the kinetic terms for the Abelian gauge fields are diagonal as

$$\mathcal{L}_{\rm kin} \supset -\frac{1}{4}\tilde{B}_{\mu\nu}\tilde{B}^{\mu\nu} - \frac{1}{4}\tilde{X}_{\mu\nu}\tilde{X}^{\mu\nu}. \tag{A.2}$$

However, the mass terms for Z boson and X boson are not diagonal on this basis as

$$\mathcal{L}_{\rm mass} \supset \frac{\hat{m}_Z^2}{2}\begin{bmatrix} \tilde{Z}_\mu & \tilde{X}_\mu \end{bmatrix} \begin{bmatrix} 1 & -\Delta \\ -\Delta & \eta^2 r_0 + \Delta^2 \end{bmatrix} \begin{bmatrix} \tilde{Z}_\mu \\ \tilde{X}_\mu \end{bmatrix}, \tag{A.3}$$

JCAP03(2024)048

where $\hat{m}_Z^2 = v^2\sqrt{g^2+g'^2}/4$ with g, g' being the gauge coupling of $\mathrm{SU(2)_L}$, $\mathrm{U(1)_Y}$, respectively, $\Delta \equiv \eta\varepsilon t_W$, and $r_0 = \hat{m}_X^2/\hat{m}_Z^2$.

The mass matrix can be diagonalized by an additional rotation matrix,

$$\begin{bmatrix} Z_\mu \\ X_\mu \end{bmatrix} = \begin{bmatrix} \cos\theta_a & -\sin\theta_a \\ \sin\theta_a & \cos\theta_a \end{bmatrix} \begin{bmatrix} \tilde{Z}_\mu \\ \tilde{X}_\mu \end{bmatrix}, \tag{A.4}$$

where θ_a is determined as

$$\begin{aligned} \tan 2\theta_a &= \frac{2\Delta}{1-\eta^2 r_0 - \Delta^2}, \\ \sin\theta_a &\approx \varepsilon t_W(1+r_0), \\ \cos\theta_a &\approx 1-\varepsilon^2 t_W^2(1+2r_0). \end{aligned} \tag{A.5}$$

B Derivation of the injected power formula

In this section, we give a detailed derivation of eq. (4.10), which we use to calculate the energy injection into the SM thermal bath. The Boltzmann equation of n_X after the resonance production can be written as

$$\dot{n}_X(t) + 3H(t)n_X(t) = -\Gamma_{\gamma\gamma\gamma}(t)n_X(t), \tag{B.1}$$

where $\Gamma_{\gamma\gamma\gamma}$ has time dependence via m_X.

The exact solution of this differential equation is simply given by

$$n_X(t) = n_X(t_i)\left(\frac{a(t_i)}{a(t)}\right)^3 \exp\left[-\int_{T(t_i)}^{T(t)} \frac{\Gamma_{\gamma\gamma\gamma}(T')}{H(T')T'}dT'\right], \tag{B.2}$$

where t_i can be arbitrary time prior to t, and $T(t)$ is the temperature at t. In this expression, $(a(t_i)/a(t))^3$ factor describes the dilution due to the expansion of the universe, while the exponential factor corresponds to the decay. Let us suppose that the decay rate is proportional to some negative power of the temperature, i.e. $\Gamma_{\gamma\gamma\gamma}/(HT) \propto T^{-\beta}$ with $\beta > 0$. In this case, the integration can be easily carried out, and the result is only sensitive to the information at t, if t and t_i are well separated. Then eq. (B.2) can be written as

$$n_X(t) \approx \exp\left[-\frac{\Gamma_{\gamma\gamma\gamma}(t)}{(\beta-1)H(t)}\right]\left(\frac{2\pi^2}{45}g_{*s}T^3\right)Y_X. \tag{B.3}$$

If m_X is in the tracking regime or the trapped regime where the exponential factor of $n_X(t)$ is close to the one, m_X as well as $\Gamma_{\gamma\gamma\gamma}$ should be proportional to some negative powers of T. The loophole of the approximation arises when i) the exponential factor of $n_X(t)$ becomes much larger than one during the trapped regime, or ii) near e^+e^- threshold where the enhancement factor $F(m_X)$ has a significant impact on the decay rate.

Nonetheless, we can use eq. (B.3) to estimate the energy injection into the SM thermal bath. In case i), the growth of the exponential factor implies that a large portion of the dark gauge boson has already decayed to the photons. Thus, the contribution of error in this regime is tiny. In case ii), the enhancement factor is important only shortly before m_X passes

JCAP03(2024)048

e^+e^- threshold. Since e^+e^- channel opens right after the threshold, energy injection can be captured by taking that the remaining energy density decays at e^+e^- threshold.

The values of β in various situations are given by

$$\beta = \begin{cases} (3\alpha+30)/(\alpha+1) & (\text{trapped},\ T > T_{\rm eq}), \\ (5\alpha+59)/(2\alpha+2) & (\text{trapped},\ T < T_{\rm eq}), \\ (3\alpha+42)/(\alpha+2) & (\text{tracking},\ T > T_{\rm eq}), \\ (5\alpha+64)/(2\alpha+4) & (\text{tracking},\ T < T_{\rm eq}). \end{cases} \tag{B.4}$$

References

[1] Supernova Search Team collaboration, *Observational evidence from supernovae for an accelerating universe and a cosmological constant*, *Astron. J.* **116** (1998) 1009 [astro-ph/9805201] [INSPIRE].

[2] Supernova Cosmology Project collaboration, *Measurements of* Ω *and* Λ *from* 42 *high redshift supernovae*, *Astrophys. J.* **517** (1999) 565 [astro-ph/9812133] [INSPIRE].

[3] C. Wetterich, *Cosmology and the fate of dilatation symmetry*, *Nucl. Phys. B* **302** (1988) 668 [arXiv:1711.03844] [INSPIRE].

[4] B. Ratra and P.J.E. Peebles, *Cosmological consequences of a rolling homogeneous scalar field*, *Phys. Rev. D* **37** (1988) 3406 [INSPIRE].

[5] P.G. Ferreira and M. Joyce, *Structure formation with a selftuning scalar field*, *Phys. Rev. Lett.* **79** (1997) 4740 [astro-ph/9707286] [INSPIRE].

[6] R.R. Caldwell, R. Dave and P.J. Steinhardt, *Cosmological imprint of an energy component with general equation of state*, *Phys. Rev. Lett.* **80** (1998) 1582 [astro-ph/9708069] [INSPIRE].

[7] R.H. Brandenberger, *Alternatives to the inflationary paradigm of structure formation*, *Int. J. Mod. Phys. Conf. Ser.* **01** (2011) 67 [arXiv:0902.4731] [INSPIRE].

[8] V.F. Mukhanov and G.V. Chibisov, *Quantum fluctuations and a nonsingular universe*, *JETP Lett.* **33** (1981) 532 [INSPIRE].

[9] H. Kodama and M. Sasaki, *Cosmological perturbation theory*, *Prog. Theor. Phys. Suppl.* **78** (1984) 1 [INSPIRE].

[10] R.A. Alpher, H. Bethe and G. Gamow, *The origin of chemical elements*, *Phys. Rev.* **73** (1948) 803 [INSPIRE].

[11] C. Hayashi, *Proton-neutron concentration ratio in the expanding universe at the stages preceding the formation of the elements*, *Prog. Theor. Phys.* **5** (1950) 224 [INSPIRE].

[12] T.P. Walker et al., *Primordial nucleosynthesis redux*, *Astrophys. J.* **376** (1991) 51 [INSPIRE].

[13] T. Damour and A.M. Polyakov, *String theory and gravity*, *Gen. Rel. Grav.* **26** (1994) 1171 [gr-qc/9411069] [INSPIRE].

[14] T. Damour and A.M. Polyakov, *The string dilaton and a least coupling principle*, *Nucl. Phys. B* **423** (1994) 532 [hep-th/9401069] [INSPIRE].

[15] M. Gasperini, F. Piazza and G. Veneziano, *Quintessence as a runaway dilaton*, *Phys. Rev. D* **65** (2002) 023508 [gr-qc/0108016] [INSPIRE].

JCAP03(2024)048

[16] K. Choi, *String or M theory axion as a quintessence*, *Phys. Rev. D* **62** (2000) 043509 [hep-ph/9902292] [INSPIRE].

[17] J.E. Kim and H.P. Nilles, *A quintessential axion*, *Phys. Lett. B* **553** (2003) 1 [hep-ph/0210402] [INSPIRE].

[18] P. Jordan, *The present state of Dirac's cosmological hypothesis*, *Z. Phys.* **157** (1959) 112 [INSPIRE].

[19] C. Brans and R.H. Dicke, *Mach's principle and a relativistic theory of gravitation*, *Phys. Rev.* **124** (1961) 925 [INSPIRE].

[20] P.G. Bergmann, *Comments on the scalar tensor theory*, *Int. J. Theor. Phys.* **1** (1968) 25 [INSPIRE].

[21] R.V. Wagoner, *Scalar tensor theory and gravitational waves*, *Phys. Rev. D* **1** (1970) 3209 [INSPIRE].

[22] E.J. Copeland, A.R. Liddle and D. Wands, *Exponential potentials and cosmological scaling solutions*, *Phys. Rev. D* **57** (1998) 4686 [gr-qc/9711068] [INSPIRE].

[23] N. Bartolo and M. Pietroni, *Scalar tensor gravity and quintessence*, *Phys. Rev. D* **61** (2000) 023518 [hep-ph/9908521] [INSPIRE].

[24] D. Comelli, M. Pietroni and A. Riotto, *Dark energy and dark matter*, *Phys. Lett. B* **571** (2003) 115 [hep-ph/0302080] [INSPIRE].

[25] J. Khoury and A. Weltman, *Chameleon fields: awaiting surprises for tests of gravity in space*, *Phys. Rev. Lett.* **93** (2004) 171104 [astro-ph/0309300] [INSPIRE].

[26] J. Khoury and A. Weltman, *Chameleon cosmology*, *Phys. Rev. D* **69** (2004) 044026 [astro-ph/0309411] [INSPIRE].

[27] P. Brax et al., *Detecting dark energy in orbit: the cosmological chameleon*, *Phys. Rev. D* **70** (2004) 123518 [astro-ph/0408415] [INSPIRE].

[28] D.F. Mota and D.J. Shaw, *Evading equivalence principle violations, cosmological and other experimental constraints in scalar field theories with a strong coupling to matter*, *Phys. Rev. D* **75** (2007) 063501 [hep-ph/0608078] [INSPIRE].

[29] T. Faulkner, M. Tegmark, E.F. Bunn and Y. Mao, *Constraining $f(R)$ gravity as a scalar tensor theory*, *Phys. Rev. D* **76** (2007) 063505 [astro-ph/0612569] [INSPIRE].

[30] K. Hinterbichler, J. Khoury, A. Levy and A. Matas, *Symmetron cosmology*, *Phys. Rev. D* **84** (2011) 103521 [arXiv:1107.2112] [INSPIRE].

[31] J. Wang, L. Hui and J. Khoury, *No-go theorems for generalized chameleon field theories*, *Phys. Rev. Lett.* **109** (2012) 241301 [arXiv:1208.4612] [INSPIRE].

[32] P. Brax, A.-C. Davis, B. Li and H.A. Winther, *A unified description of screened modified gravity*, *Phys. Rev. D* **86** (2012) 044015 [arXiv:1203.4812] [INSPIRE].

[33] K. Kaneta, K.-Y. Oda and M. Yoshimura, *Constraints on extended Jordan-Brans-Dicke gravity*, *JCAP* **10** (2023) 040 [arXiv:2304.08656] [INSPIRE].

[34] PLANCK collaboration, *Planck* 2018 *results. VI. Cosmological parameters*, *Astron. Astrophys.* **641** (2020) A6 [*Erratum ibid.* **652** (2021) C4] [arXiv:1807.06209] [INSPIRE].

[35] I. Zlatev, L.-M. Wang and P.J. Steinhardt, *Quintessence, cosmic coincidence, and the cosmological constant*, *Phys. Rev. Lett.* **82** (1999) 896 [astro-ph/9807002] [INSPIRE].

JCAP03(2024)048

[36] K. Kaneta, H.-S. Lee, J. Lee and J. Yi, *Gauged quintessence*, *JCAP* **02** (2023) 005 [arXiv:2208.09229] [INSPIRE].

[37] K. Kaneta, H.-S. Lee, J. Lee and J. Yi, *Misalignment mechanism for a mass-varying vector boson*, *JCAP* **09** (2023) 017 [arXiv:2306.01291] [INSPIRE].

[38] A. Banerjee et al., *Hubble sinks in the low-redshift swampland*, *Phys. Rev. D* **103** (2021) L081305 [arXiv:2006.00244] [INSPIRE].

[39] B.-H. Lee et al., *Is local H_0 at odds with dark energy EFT?*, *JCAP* **04** (2022) 004 [arXiv:2202.03906] [INSPIRE].

[40] A.E. Nelson and J. Scholtz, *Dark light, dark matter and the misalignment mechanism*, *Phys. Rev. D* **84** (2011) 103501 [arXiv:1105.2812] [INSPIRE].

[41] S.M. Carroll, *Quintessence and the rest of the world*, *Phys. Rev. Lett.* **81** (1998) 3067 [astro-ph/9806099] [INSPIRE].

[42] D.J. Shaw, *Charge non-conservation, dequantisation, and induced electric dipole moments in varying-alpha theories*, *Phys. Lett. B* **632** (2006) 105 [hep-th/0509093] [INSPIRE].

[43] F. Ferlito, S. Vagnozzi, D.F. Mota and M. Baldi, *Cosmological direct detection of dark energy: non-linear structure formation signatures of dark energy scattering with visible matter*, *Mon. Not. Roy. Astron. Soc.* **512** (2022) 1885 [arXiv:2201.04528] [INSPIRE].

[44] S. Vagnozzi et al., *Direct detection of dark energy: the XENON1T excess and future prospects*, *Phys. Rev. D* **104** (2021) 063023 [arXiv:2103.15834] [INSPIRE].

[45] K.V. Berghaus et al., *Dark energy radiation*, *Phys. Rev. D* **104** (2021) 083520 [arXiv:2012.10549] [INSPIRE].

[46] K.V. Berghaus, T. Karwal, V. Miranda and T. Brinckmann, *The cosmology of dark energy radiation*, arXiv:2311.08638 [INSPIRE].

[47] P. Brax, C. van de Bruck and A.-C. Davis, *Compatibility of the chameleon-field model with fifth-force experiments, cosmology, and PVLAS and CAST results*, *Phys. Rev. Lett.* **99** (2007) 121103 [hep-ph/0703243] [INSPIRE].

[48] P. Brax et al., *Testing chameleon theories with light propagating through a magnetic field*, *Phys. Rev. D* **76** (2007) 085010 [arXiv:0707.2801] [INSPIRE].

[49] K. Homma and Y. Kirita, *Stimulated radar collider for probing gravitationally weak coupling pseudo Nambu-Goldstone bosons*, *JHEP* **09** (2020) 095 [arXiv:1909.00983] [INSPIRE].

[50] S. Vagnozzi, L. Visinelli, O. Mena and D.F. Mota, *Do we have any hope of detecting scattering between dark energy and baryons through cosmology?*, *Mon. Not. Roy. Astron. Soc.* **493** (2020) 1139 [arXiv:1911.12374] [INSPIRE].

[51] P. Brax et al., *Collider constraints on interactions of dark energy with the Standard Model*, *JHEP* **09** (2009) 128 [arXiv:0904.3002] [INSPIRE].

[52] P. Brax et al., *Higgs production as a probe of chameleon dark energy*, *Phys. Rev. D* **81** (2010) 103524 [arXiv:0911.1267] [INSPIRE].

[53] P. Brax, C. Burrage and C. Englert, *Disformal dark energy at colliders*, *Phys. Rev. D* **92** (2015) 044036 [arXiv:1506.04057] [INSPIRE].

[54] P. Brax, C. Burrage, C. Englert and M. Spannowsky, *LHC signatures of scalar dark energy*, *Phys. Rev. D* **94** (2016) 084054 [arXiv:1604.04299] [INSPIRE].

JCAP03(2024)048

[55] ATLAS collaboration, *Constraints on mediator-based dark matter and scalar dark energy models using $\sqrt{s} = 13$ TeV pp collision data collected by the ATLAS detector*, *JHEP* **05** (2019) 142 [arXiv:1903.01400] [INSPIRE].

[56] J.A. Casas, J. Garcia-Bellido and M. Quiros, *Scalar-tensor theories of gravity with phi dependent masses*, *Class. Quant. Grav.* **9** (1992) 1371 [hep-ph/9204213] [INSPIRE].

[57] J. Garcia-Bellido, *Dark matter with variable masses*, *Int. J. Mod. Phys. D* **2** (1993) 85 [hep-ph/9205216] [INSPIRE].

[58] G.W. Anderson and S.M. Carroll, *Dark matter with time dependent mass*, in the proceedings of the 1st *International Conference on Particle Physics and the Early Universe*, (1997) [DOI:10.1142/9789814447263_0025] [astro-ph/9711288] [INSPIRE].

[59] R. Fardon, A.E. Nelson and N. Weiner, *Dark energy from mass varying neutrinos*, *JCAP* **10** (2004) 005 [astro-ph/0309800] [INSPIRE].

[60] A. Berlin and D. Hooper, *Axion-assisted production of sterile neutrino dark matter*, *Phys. Rev. D* **95** (2017) 075017 [arXiv:1610.03849] [INSPIRE].

[61] G. Krnjaic, P.A.N. Machado and L. Necib, *Distorted neutrino oscillations from time varying cosmic fields*, *Phys. Rev. D* **97** (2018) 075017 [arXiv:1705.06740] [INSPIRE].

[62] H. Davoudiasl and G. Mohlabeng, *Getting a THUMP from a WIMP*, *JHEP* **04** (2020) 177 [arXiv:1912.05572] [INSPIRE].

[63] L. Boubekeur and S. Profumo, *Tremaine-Gunn limit with mass-varying particles*, *Phys. Rev. D* **107** (2023) 103535 [arXiv:2302.10246] [INSPIRE].

[64] Y.L. ChoeJo, Y. Kim and H.-S. Lee, *Dirac-Majorana neutrino type oscillation induced by a wave dark matter*, *Phys. Rev. D* **108** (2023) 095028 [arXiv:2305.16900] [INSPIRE].

[65] Y.L. ChoeJo, K. Enomoto, Y. Kim and H.-S. Lee, *Second leptogenesis: unraveling the baryon-lepton asymmetry discrepancy*, *JHEP* **03** (2024) 003 [arXiv:2311.16672] [INSPIRE].

[66] B. Holdom, *Two* U(1)*'s and epsilon charge shifts*, *Phys. Lett. B* **166** (1986) 196 [INSPIRE].

[67] T. Altherr and U. Kraemmer, *Gauge field theory methods for ultradegenerate and ultrarelativistic plasmas*, *Astropart. Phys.* **1** (1992) 133 [INSPIRE].

[68] E. Braaten and D. Segel, *Neutrino energy loss from the plasma process at all temperatures and densities*, *Phys. Rev. D* **48** (1993) 1478 [hep-ph/9302213] [INSPIRE].

[69] J. Redondo, *Helioscope bounds on hidden sector photons*, *JCAP* **07** (2008) 008 [arXiv:0801.1527] [INSPIRE].

[70] J. Redondo and M. Postma, *Massive hidden photons as lukewarm dark matter*, *JCAP* **02** (2009) 005 [arXiv:0811.0326] [INSPIRE].

[71] P.J. Steinhardt, L.-M. Wang and I. Zlatev, *Cosmological tracking solutions*, *Phys. Rev. D* **59** (1999) 123504 [astro-ph/9812313] [INSPIRE].

[72] A.D. Linde, *Phase transitions in gauge theories and cosmology*, *Rept. Prog. Phys.* **42** (1979) 389 [INSPIRE].

[73] K. Kaneta, H.-S. Lee and S. Yun, *Portal connecting dark photons and axions*, *Phys. Rev. Lett.* **118** (2017) 101802 [arXiv:1611.01466] [INSPIRE].

[74] K. Kaneta, H.-S. Lee and S. Yun, *Dark photon relic dark matter production through the dark axion portal*, *Phys. Rev. D* **95** (2017) 115032 [arXiv:1704.07542] [INSPIRE].

JCAP03(2024)048

[75] M. Escudero Abenza, *Precision early universe thermodynamics made simple: $N_{\rm eff}$ and neutrino decoupling in the Standard Model and beyond*, *JCAP* **05** (2020) 048 [arXiv:2001.04466] [INSPIRE].

[76] L.C. Thomas, T. Dezen, E.B. Grohs and C.T. Kishimoto, *Electron-positron annihilation freeze-out in the early universe*, *Phys. Rev. D* **101** (2020) 063507 [arXiv:1910.14050] [INSPIRE].

[77] M. Ibe, S. Kobayashi, Y. Nakayama and S. Shirai, *Cosmological constraint on dark photon from $N_{\rm eff}$*, *JHEP* **04** (2020) 009 [arXiv:1912.12152] [INSPIRE].

[78] M. Pospelov, A. Ritz and M.B. Voloshin, *Bosonic super-WIMPs as keV-scale dark matter*, *Phys. Rev. D* **78** (2008) 115012 [arXiv:0807.3279] [INSPIRE].

[79] S.D. McDermott, H.H. Patel and H. Ramani, *Dark photon decay beyond the Euler-Heisenberg limit*, *Phys. Rev. D* **97** (2018) 073005 [arXiv:1705.00619] [INSPIRE].

[80] J. Jaeckel, J. Redondo and A. Ringwald, *Signatures of a hidden cosmic microwave background*, *Phys. Rev. Lett.* **101** (2008) 131801 [arXiv:0804.4157] [INSPIRE].

[81] J.D. Bjorken, R. Essig, P. Schuster and N. Toro, *New fixed-target experiments to search for dark gauge forces*, *Phys. Rev. D* **80** (2009) 075018 [arXiv:0906.0580] [INSPIRE].

[82] J.H. Chang, R. Essig and S.D. McDermott, *Revisiting supernova 1987A constraints on dark photons*, *JHEP* **01** (2017) 107 [arXiv:1611.03864] [INSPIRE].

[83] W. DeRocco et al., *Observable signatures of dark photons from supernovae*, *JHEP* **02** (2019) 171 [arXiv:1901.08596] [INSPIRE].

[84] N. Arkani-Hamed, L. Motl, A. Nicolis and C. Vafa, *The string landscape, black holes and gravity as the weakest force*, *JHEP* **06** (2007) 060 [hep-th/0601001] [INSPIRE].

[85] B. Heidenreich, M. Reece and T. Rudelius, *Evidence for a sublattice weak gravity conjecture*, *JHEP* **08** (2017) 025 [arXiv:1606.08437] [INSPIRE].

[86] B. Heidenreich, M. Reece and T. Rudelius, *The weak gravity conjecture and emergence from an ultraviolet cutoff*, *Eur. Phys. J. C* **78** (2018) 337 [arXiv:1712.01868] [INSPIRE].

[87] T. Gherghetta, J. Kersten, K. Olive and M. Pospelov, *Evaluating the price of tiny kinetic mixing*, *Phys. Rev. D* **100** (2019) 095001 [arXiv:1909.00696] [INSPIRE].

[88] W. Hu and J. Silk, *Thermalization and spectral distortions of the cosmic background radiation*, *Phys. Rev. D* **48** (1993) 485 [INSPIRE].

[89] D.J. Fixsen et al., *The cosmic microwave background spectrum from the full COBE FIRAS data set*, *Astrophys. J.* **473** (1996) 576 [astro-ph/9605054] [INSPIRE].

[90] F. Bianchini and G. Fabbian, *CMB spectral distortions revisited: a new take on μ distortions and primordial non-Gaussianities from FIRAS data*, *Phys. Rev. D* **106** (2022) 063527 [arXiv:2206.02762] [INSPIRE].

[91] J. Chluba, *Green's function of the cosmological thermalization problem*, *Mon. Not. Roy. Astron. Soc.* **434** (2013) 352 [arXiv:1304.6120] [INSPIRE].

[92] J. Chluba and D. Jeong, *Teasing bits of information out of the CMB energy spectrum*, *Mon. Not. Roy. Astron. Soc.* **438** (2014) 2065 [arXiv:1306.5751] [INSPIRE].

[93] J. Chluba, *Green's function of the cosmological thermalization problem — II. Effect of photon injection and constraints*, *Mon. Not. Roy. Astron. Soc.* **454** (2015) 4182 [arXiv:1506.06582] [INSPIRE].

JCAP03(2024)048

[94] J. Chluba, *Which spectral distortions does ΛCDM actually predict?*, *Mon. Not. Roy. Astron. Soc.* **460** (2016) 227 [arXiv:1603.02496] [INSPIRE].

[95] K.C. Gendreau et al., *Asca observations of the spectrum of the X-ray background*, *Publ. Astron. Soc. Jpn.* **47** (1995) L5.

[96] S.C. Kappadath, *Measurement of the cosmic diffuse gamma-ray spectrum from* 800 *keV to* 30 *MeV*, Ph.D. thesis, University of New Hampshire, Durham, NH, U.S.A. (1998).

[97] D.E. Gruber, J.L. Matteson, L.E. Peterson and G.V. Jung, *The spectrum of diffuse cosmic hard X-rays measured with HEAO-1*, *Astrophys. J.* **520** (1999) 124 [astro-ph/9903492] [INSPIRE].

[98] A.W. Strong, I.V. Moskalenko and O. Reimer, *Diffuse galactic continuum gamma rays. A model compatible with EGRET data and cosmic-ray measurements*, *Astrophys. J.* **613** (2004) 962 [astro-ph/0406254] [INSPIRE].

[99] L. Bouchet et al., *INTEGRAL SPI all-sky view in soft gamma rays: study of point source and galactic diffuse emissions*, *Astrophys. J.* **679** (2008) 1315 [arXiv:0801.2086] [INSPIRE].

[100] M. Ajello et al., *Cosmic X-ray background and earth albedo spectra with Swift/BAT*, *Astrophys. J.* **689** (2008) 666 [arXiv:0808.3377] [INSPIRE].

[101] FERMI-LAT collaboration, *Fermi-LAT observations of the diffuse gamma-ray emission: implications for cosmic rays and the interstellar medium*, *Astrophys. J.* **750** (2012) 3 [arXiv:1202.4039] [INSPIRE].

[102] E. Masso and R. Toldra, *Photon spectrum produced by the late decay of a cosmic neutrino background*, *Phys. Rev. D* **60** (1999) 083503 [astro-ph/9903397] [INSPIRE].

[103] K. Abazajian, G.M. Fuller and W.H. Tucker, *Direct detection of warm dark matter in the X-ray*, *Astrophys. J.* **562** (2001) 593 [astro-ph/0106002] [INSPIRE].

[104] A. Boyarsky, A. Neronov, O. Ruchayskiy and M. Shaposhnikov, *Constraints on sterile neutrino as a dark matter candidate from the diffuse X-ray background*, *Mon. Not. Roy. Astron. Soc.* **370** (2006) 213 [astro-ph/0512509] [INSPIRE].

[105] G. Bertone, W. Buchmuller, L. Covi and A. Ibarra, *Gamma-rays from decaying dark matter*, *JCAP* **11** (2007) 003 [arXiv:0709.2299] [INSPIRE].

[106] R. Essig et al., *Constraining light dark matter with diffuse X-ray and gamma-ray observations*, *JHEP* **11** (2013) 193 [arXiv:1309.4091] [INSPIRE].

[107] H. An, M. Pospelov, J. Pradler and A. Ritz, *Direct detection constraints on dark photon dark matter*, *Phys. Lett. B* **747** (2015) 331 [arXiv:1412.8378] [INSPIRE].

[108] H. Yuksel and M.D. Kistler, *Circumscribing late dark matter decays model independently*, *Phys. Rev. D* **78** (2008) 023502 [arXiv:0711.2906] [INSPIRE].

[109] PAMELA collaboration, *An anomalous positron abundance in cosmic rays with energies* 1.5–100 *GeV*, *Nature* **458** (2009) 607 [arXiv:0810.4995] [INSPIRE].

[110] FERMI-LAT collaboration, *Measurement of separate cosmic-ray electron and positron spectra with the Fermi Large Area Telescope*, *Phys. Rev. Lett.* **108** (2012) 011103 [arXiv:1109.0521] [INSPIRE].

[111] AMS collaboration, *First result from the Alpha Magnetic Spectrometer on the International Space Station: precision measurement of the positron fraction in primary cosmic rays of* 0.5–350 *GeV*, *Phys. Rev. Lett.* **110** (2013) 141102 [INSPIRE].

JCAP03(2024)048

[112] H.E.S.S. collaboration, *Contributions of the High Energy Stereoscopic System (H.E.S.S.) to the 35th International Cosmic Ray Conference (ICRC), Busan, Korea*, arXiv:1709.06442 [INSPIRE].

[113] DAMPE collaboration, *Direct detection of a break in the teraelectronvolt cosmic-ray spectrum of electrons and positrons*, *Nature* **552** (2017) 63 [arXiv:1711.10981] [INSPIRE].

[114] CALET collaboration, *Energy spectrum of cosmic-ray electron and positron from 10 GeV to 3 TeV observed with the calorimetric electron telescope on the International Space Station*, *Phys. Rev. Lett.* **119** (2017) 181101 [arXiv:1712.01711] [INSPIRE].

[115] A.M. Hillas, *The origin of ultrahigh-energy cosmic rays*, *Ann. Rev. Astron. Astrophys.* **22** (1984) 425 [INSPIRE].

[116] H. Davoudiasl, H.-S. Lee and W.J. Marciano, *'Dark' Z implications for parity violation, rare meson decays, and Higgs physics*, *Phys. Rev. D* **85** (2012) 115019 [arXiv:1203.2947] [INSPIRE].

[117] H. Davoudiasl, H.-S. Lee and W.J. Marciano, *Muon $g-2$, rare kaon decays, and parity violation from dark bosons*, *Phys. Rev. D* **89** (2014) 095006 [arXiv:1402.3620] [INSPIRE].

[118] H. Davoudiasl et al., *Searching for new physics effects in future W mass and $\sin^2\theta_W(Q^2)$ determinations*, *Phys. Rev. D* **108** (2023) 115018 [arXiv:2309.04060] [INSPIRE].

JCAP03(2024)048